

Theoretical Study of Vibrationally Averaged Dipole Moments for the Ground and Excited C=O Stretching States of *trans*-Formic Acid

Leif O. Paulson,[†] Jakub Kaminský,[‡] David T. Anderson,[†] Petr Bouř,^{*,‡} and Jan Kubelka^{*,†}

Department of Chemistry, University of Wyoming, Laramie, Wyoming 82071, and Institute for Organic Chemistry and Biochemistry, Academy of Sciences of the Czech Republic, Flemingovo nám. 2, 16610, Prague, Czech Republic

Received September 12, 2009

Abstract: Recent experimental studies of *trans*-formic acid (FA) in solid para-hydrogen (pH₂) highlighted the importance of vibrationally averaged dipole moments for the interpretation of the high-resolution infrared (IR) spectra, in particular for the C=O stretch (ν_3) mode. In this report, dipole moments for the ν_3 ground ($v = 0$) and excited ($v = 1, 2, 3$, and 4) anharmonic vibrational states in *trans*-FA are investigated using two different approaches: a single mode approximation, where the vibrational states are obtained from the solution of the one-dimensional Schrödinger equation for the harmonic normal coordinate, and a limited vibrational configuration interaction (VCI) approximation. Density functional theory (B3LYP, BPW91) and correlated ab initio (MP2 and CCSD(T)) electronic methods were employed with a number of double- and triple- ζ and correlation consistent basis sets. Both single mode and VCI approaches show comparable agreement with experimental data, which is more dependent on the level of theory used. In particular, the BPW91/cc-pVDZ level appears to perform remarkably well. Effects of solvation of FA in solid state Ar and pH₂ matrices were simulated at the BPW91/cc-pVDZ level using a conductor-like polarized continuum model (CPCM). The Ar and pH₂ solid-state matrices cause quite a substantial increase in the FA dipole moments. Compared to gas-phase calculations, the CPCM model for pH₂ better reproduces the experimental FA spectral shifts caused by interaction with traces of ortho-hydrogen (oH₂) species in solid pH₂. The validity of the single mode approach is tested against the multidimensional VCI results, suggesting that the isolated (noninteracting) mode approximation is valid up to the third vibrationally excited state ($v = 3$). Finally, the contribution of the ground anharmonic vibrational states of the remaining modes to the resulting ν_3 single mode dipole moments is examined and discussed.

1. Introduction

Electrostatic forces are responsible for the structure of molecules and complexes, their spectroscopic detection, and intermolecular interactions.^{1,2} Since an overwhelming majority of molecules are polar, electric dipole moments dominate

in interactions with electric fields and form a basis for the most fundamental models of the condensed phases.³ Solute–solvent electrostatic interactions can have profound effects on the properties of studied molecules, including their spectroscopic signatures,⁴ which provide insight into the properties of both the studied solute species and the surrounding solvent.⁵

Formic acid (FA) is a prototypical, highly polar molecule, which has been subject to numerous vibrational spectroscopic investigations in the gas phase,^{6–10} solution, and several low-

* To whom correspondence should be addressed. E-mail: bour@uochab.cas.cz (P.B.); jkubelka@uwyo.edu (J.K.).

[†] University of Wyoming.

[‡] Academy of Sciences of the Czech Republic.

temperature matrix isolation host materials.^{11–18} In our recent study of *trans*-FA in low temperature para-H₂ (pH₂) matrices using high-resolution FTIR spectroscopy,¹⁸ we observed multiple closely spaced peaks for the C=O stretching fundamental, commonly denoted as ν_3 ,¹⁰ as well as for the $2\nu_3$ overtone band. We proposed that these multiplets arise from preferential clustering of the quadrupolar ortho-H₂ (oH₂) species, which is always present in ppm concentrations in the pH₂ matrix, to the FA dopant molecule. The electrostatic interaction between the oH₂ quadrupole moment and the dipole moments of FA in the ground and excited ν_3 vibrational states causes the splitting of the FA ν_3 absorption.

Quantitative explanation of these spectral features requires the value of the molecular dipole moment of FA in the ν_3 ground and vibrationally excited states. While for the ground and the first ν_3 excited state the dipole moments have been experimentally measured,⁸ they have not been reported for higher excited states. Furthermore, no experimental dipole moment data are available for FA in any solid matrix environment. Since the solvent, or matrix, can have pronounced effects on the vibrational frequencies and intensities, especially those associated with polar bonds such as C=O,^{19–24} it is likely that the permanent dipole moments will also be sensitive to the solvent or matrix environment. In this report, we present theoretical calculations of the vibrationally averaged dipole moments for the ground and excited states of the ν_3 vibrational mode of FA in the gas phase, as well as in an Ar and pH₂ matrix environment, treated by an implicit polarized continuum model.

Theoretical determination of the vibrationally averaged dipole moments necessitates accurate modeling of the anharmonic vibrational states. Unfortunately, no universal approach exists for obtaining vibrational properties of sizable molecules beyond the harmonic limit.²⁵ In this study, two different approaches are explored. The first is based on a one-dimensional (1D) anharmonic vibrational energy and dipole moment function calculated for the ν_3 normal mode of the FA. The normal mode coordinate is treated as independent from all other vibrational degrees of freedom. This approach is analogous to the simple local mode model,²⁶ which has proven very useful in the investigations of overtone vibrations involving predominantly X–H stretching,^{27,28} including the O–H stretch of FA.^{9,29,30} Since our treatment is based on the normal mode, we use the term “single mode method” to distinguish this approach from the conceptually different local mode theory of molecular vibrations.^{31–33} The second approach is a multidimensional limited vibrational configuration interaction (VCI) methodology,^{25,34} which includes all vibrational coordinates. A third approach, the multidimensional degeneration-corrected second-order perturbation theory,²⁵ was also tested with very similar results to those obtained by VCI, as observed previously for other vibrationally averaged properties.³⁵

2. Computational Methods

2.1. Single Mode Model. In the single mode picture²⁶ the vibrational states (wave functions) are found as solutions to the 1D Schrödinger equation:

$$\left[-\frac{\hbar^2}{2m} \frac{d^2}{dR^2} + V(R) \right] \psi(R) = E\psi(R) \quad (1)$$

where m is the reduced mass and $V(R)$ is the potential energy as a function of the ν_3 normal coordinate R . We use the symbol “ R ” for the non-mass-weighted normal coordinate, to distinguish it from the mass-weighted normal coordinates (Q) used in the next section. R and m were obtained from harmonic vibrational calculations using the Gaussian 98/03 quantum chemistry package.³⁶ Density functional theory (DFT, B3LYP, and BPW91 functionals) and correlated ab initio [MP2 and CCSD(T)] methods were employed along with a number of basis sets (see Results). The effects of the solid-state Ar and pH₂ matrices were simulated using the conductor polarized continuum model (CPCM)^{37,38} with the dielectric constant $\epsilon = 1.43$ for Ar and $\epsilon = 1.294$ for pH₂.³⁹ Additional CPCM parameters (default in Gaussian 03) were the united atom (UA0) topological model for the solute radii (2.125, 1.75, and 1.85 Å radii for the CH, O and OH groups, respectively), the solvent radius of 1.875 Å, and the average tesserae area of 0.2 Å².

At each level of theory, the FA geometry was fully optimized, followed by a harmonic vibrational frequency calculation. The optimized geometries are listed and compared to available experimental data in Supporting Information, Table S1. Energies $V(R)$ and dipole moments $\mu(R)$ were computed for a series of 49 structures [25 structures for CCSD(T)/aug-cc-pVTZ level] generated at discrete steps along the ν_3 normal mode displacement R . The points were quadratically distributed from -0.35 to $+1.0$ Å with respect to the energy minimum to ensure adequate sampling of the potential near its maximum curvature. Gaussian was used for all calculations except CCSD(T), for which the population analysis is not implemented and the energy surfaces and dipole moments were calculated using ACESII.⁴⁰

The Schrödinger equation (eq 2) for the resulting potential energy profile was solved numerically using the grid variational method^{41,42} with MATLAB (Mathworks Inc. Mattick, MA) codes written in-house. The wave function was expanded as a linear combination of coordinate grid points $|r_i\rangle$:

$$|\psi(R)\rangle = \sum_{i=1}^{N_{\text{grid}}} \psi(r_i) |r_i\rangle \quad (2)$$

Substituting eq 2 into 3 and applying the standard variational principle with respect to $\psi(r_i)$ subject to the normalization constraint lead to the following system of linear equations

$$\sum_{j=1}^{N_{\text{grid}}} (H_{ij} - E\delta_{ij})\psi(r_j) = 0 \quad (3)$$

where

$$H_{ij} = \langle r_i | -\frac{\hbar^2}{2m} \frac{d^2}{dr^2} + V(r) | r_j \rangle \quad (4)$$

The grid consisted of 401 points from $r_{\text{eq}} - 0.3 \text{ \AA}$ to $r_{\text{eq}} + 0.5 \text{ \AA}$. A fifth-order finite difference method was used for the second derivative:

$$\langle r_i | \frac{d^2}{dr^2} | r_j \rangle = \frac{1}{\Delta r^2} \left[-\frac{5269}{1800} \delta_{ij} + \frac{5}{3} \delta_{i\pm 1,j} - \frac{5}{21} \delta_{i\pm 2,j} + \frac{5}{126} \delta_{i\pm 3,j} - \frac{5}{1008} \delta_{i\pm 4,j} + \frac{1}{3150} \delta_{i\pm 5,j} \right] \quad (5)$$

The potential energy is diagonal, i.e. $\langle r_i | V(r_i) | r_j \rangle = V(r_i) \delta_{ij}$; values of $V(r_i)$ at the individual grid points were interpolated from 40 single-point Gaussian energies (above). The five lowest eigenvalues and eigenvectors of the Hamiltonian matrix (eq 5), corresponding to the vibrational states $v = 0, 1, 2, 3$ and 4, were calculated using iterative sparse matrix methods as implemented in MATLAB. Vibrationally averaged dipole moments were obtained as

$$\boldsymbol{\mu}_v = \langle \psi_v(R) | \boldsymbol{\mu}(R) | \psi_v(R) \rangle = \sum_{i=1}^{N_{\text{grid}}} \psi_v(r_i) \boldsymbol{\mu}(r_i) \psi_v(r_i) \quad (6)$$

The dipole moments at the grid points $\boldsymbol{\mu}(r_i)$ were again interpolated from the values obtained from the quantum mechanical calculations.

2.2. Multidimensional Anharmonic Calculations. All vibrational degrees of freedom were considered in the Taylor expansion of the potential in the (mass weighted) normal mode coordinates Q_i up to the fourth order:

$$V(Q_1, \dots, Q_M) = \sum_{i=1}^M \frac{\omega_i^2}{2} Q_i^2 + \frac{1}{6} \sum_{i=1}^M \sum_{j=1}^M \sum_{k=1}^M c_{ijk} Q_i Q_j Q_k + \frac{1}{24} \sum_{i=1}^M \sum_{j=1}^M \sum_{k=1}^M \sum_{l=1}^M d_{ijkl} Q_i Q_j Q_k Q_l + \dots \quad (7)$$

where all cubic and semidiagonal normal mode quartic constants (i.e., with two and more identical indices, such as d_{ijkk}) were considered, obtainable by back and forth normal-mode numerical differentiation of harmonic force fields; ω_i are the harmonic frequencies and $M = 3 \times$ number of atoms $- 6$. The harmonic force fields were obtained from Gaussian³⁶ at four levels of theory: B3LYP/6-311++G(d,p), BPW91/cc-pVDZ, MP2/6-311++G(d,p), and CCSD(T)/6-311++G(d,p). As for the single mode method, Ar and pH₂ matrices were included at BPW91/cc-pVDZ level by CPCM solvent model, with the same parameters as detailed above. The program S4^{43,44} was used for the anharmonic computations, enabling vibrational configuration interaction (VCI) within the harmonic oscillator basis functions. To limit the size of the VCI Hamiltonian, the harmonic basis was restricted to the ground and first five excited state wave functions. The effects of the size of the harmonic basis including up to seven excited states were tested for the BPW91/cc-pVDZ level calculations (Supporting Information, Table S3).

The dipole moment $\boldsymbol{\mu}_v$ was calculated from the VCI wave function ψ_v for each selected state v as a quantum average

$$\boldsymbol{\mu}_v = \langle \psi_v | \boldsymbol{\mu} | \psi_v \rangle \quad (8)$$

where the molecular dipole moment $\boldsymbol{\mu}$ was expanded as

$$\boldsymbol{\mu}_\beta = \mu_{0,\beta} + \sum_i P_{\beta,i} Q_i + \frac{1}{2} \sum_{ij} D_{\beta,ij} Q_i Q_j \quad (9)$$

where $\beta = \{x, y, z\}$ and \mathbf{P} are the first and \mathbf{D} the second normal mode dipole derivatives. The tensor \mathbf{P} was obtained from the Cartesian dipole derivatives $\boldsymbol{\Pi}$ (atomic polar tensors) as

$$P_{\beta,i} = \sum_{\lambda,\alpha} \Pi_{\beta,\lambda\alpha} S_{\lambda\alpha,i} \quad (10)$$

where \mathbf{S} is the normal mode–Cartesian transformation matrix. The second derivatives \mathbf{D} were obtained in normal modes from \mathbf{P} , using a two-step differentiation formula,

$$D_{\beta,ij} = \frac{P_{\beta,i}(Q_j + \Delta) - P_{\beta,i}(Q_j - \Delta)}{2\Delta} \quad (11)$$

with $\Delta = 0.0022$ au for the CCSD(T) computation; however, the first ($P_{\beta,i}$) and diagonal second ($D_{\beta,ij}$ with $i = j$) dipole derivatives were obtained from a two-step numerical differentiation of dipoles at CCD/6-311++G(d,p) level; the off-diagonal second dipole derivatives ($D_{\beta,ij}$ with $i \neq j$) were neglected in this case.

3. Results

3.1. Single Mode Approximation. A typical one-dimensional (1D) potential and dipole moment function for the ν_3 normal mode (calculated at BPW91/cc-pVDZ level) are shown in Figure 1a. Potential energy and dipole moment functions for additional levels of theory are shown in the Supporting Information (Figure S1). The corresponding solutions of the 1-D Schrödinger equation (eq 1) for $v = 0-4$ are shown in Figure 1b. From these solutions, the vibrational parameters, frequencies, and spectral intensities, as well as the vibrationally averaged dipole moments, were obtained as detailed in the Computational Methods.

The computed vibrationally averaged dipole moments, along with the equilibrium structure values and available experimental data, are shown in Table 1. To highlight the resulting trends, the vibrationally averaged dipole moments are also plotted in Figure 2. All calculations predict the dipole moment to increase with the vibrational excitation, in agreement with the available experimental data for the ground and the first excited states. In all cases, the ground vibrational state dipole moment is greater than that for the minimum structure. The DFT methods generally overestimate the dipole moments, in particular with the augmented correlation consistent basis sets. The exception is the ground-state dipole computed with BPW91/cc-pVDZ, which is slightly lower (by ~ 0.002 D) than the experimental value and in the best overall agreement. The first vibrationally excited state dipole moments are without exception computed too high and generally with larger error than the ground state ones. The closest to experiment is again BPW91/cc-pVDZ, yielding a ~ 0.012 D greater value. The post-HF methods uniformly predict lower dipole moments than DFT with the same basis sets, but similar trends with respect to the basis

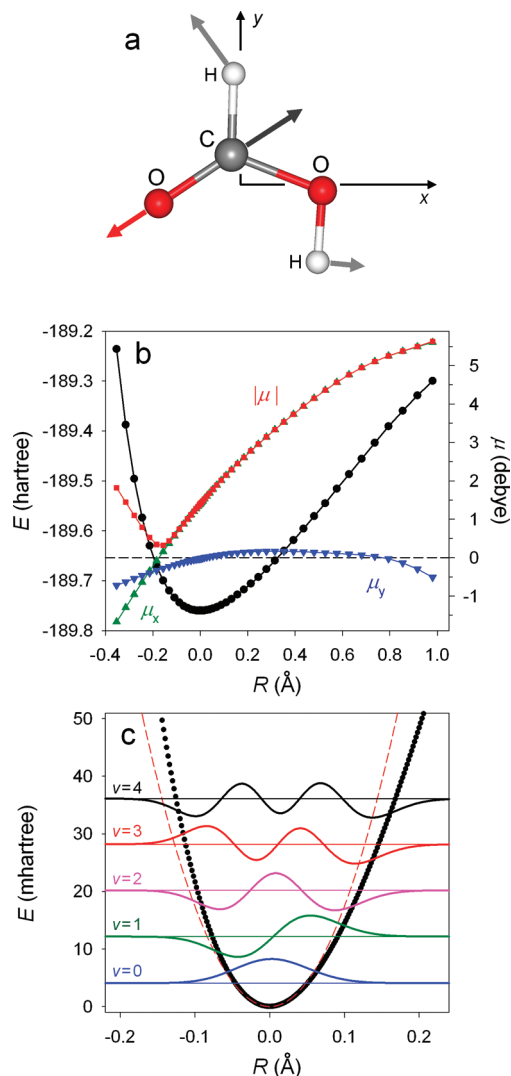


Figure 1. One-dimensional single mode representation of the ν_3 vibration in *trans*-FA. (a) The ν_3 normal mode of *trans*-FA. The molecule is oriented in the x - y plane, with axes parallel to the principal axes of the moment of inertia. The coordinate origin is at the center of nuclear charge. (b) Potential energy (black circles), the dipole moment components (x , green triangles; y , blue triangles), and magnitude (red squares) calculated at BPW91/cc-pVDZ level as functions of the ν_3 normal mode coordinate (R). (c) Solutions of the 1D Schrödinger equation for the potential energy function from part a shown as black circles. The dashed red line is the harmonic potential.

set size and type are observed. Namely, diffuse basis functions generally increase the computed dipole moments and augmented correlation consistent basis sets yield greater dipole values than 6-311++G(d,p). As a consequence, MP2 and CCSD(T) with the smaller basis sets severely underestimate the experimental dipole moments; however, the agreement improves with larger basis sets, in contrast to DFT. In particular, the CCSD(T)/aug-cc-pVTZ ground vibrational state dipole moment is in very good agreement with experiment (~ 0.005 D lower).

CPCM calculations for Ar and pH_2 matrices with BPW91/cc-pVDZ show a significant increase in the dipole moments with respect to the gas phase. The ground-state dipole moment in Ar is calculated to increase by ~ 0.16 D and in

pH_2 matrix by ~ 0.11 D. A similar relative increase with respect to the gas phase is computed for all vibrationally excited states, the differences getting slightly smaller for higher ν . These large matrix effects may seem somewhat surprising, given the rather subtle changes in FA geometry and vibrational frequencies (Supporting Information, Tables S1 and S6), but they are consistent with the increase in the spectral intensity (Supporting Information, Table S7).

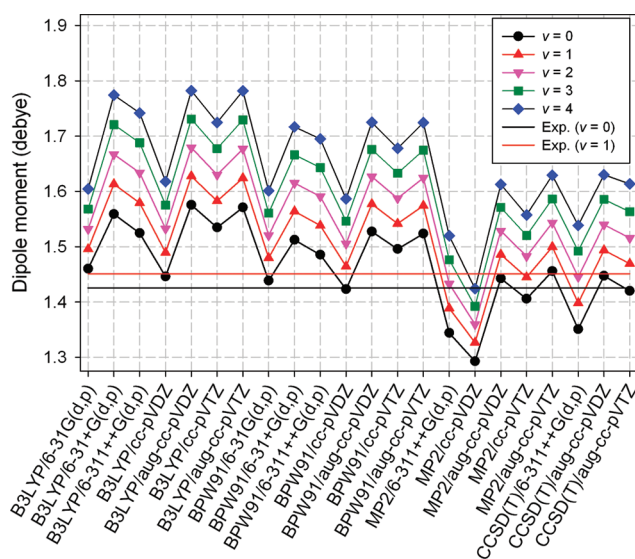
As apparent from Figure 2, despite a wide variation in the dipole moments computed at various levels of theory, there is a systematic increase in the dipole moment with the vibrational state. It is therefore interesting to explore the changes in the computed excited state ($\nu = 1, 2, 3$, and 4) dipole moments with respect to the ground state ($\nu = 0$) as shown in Figure 3. The computed changes are systematically greater than the only available experimental reference (for $\nu = 1$), but more severe overestimation can be expected for the higher excited states. While the difference dipole moments are more consistent among all the methods, similar trends as those observed for the absolute values are still apparent: methods that gave higher absolute dipole moments also tend to give higher increments in the vibrationally excited states (Table 1, Figure 2). However, comparison of the dipole moment differences more clearly highlights the effects of basis sets. As evident from Figure 3, the same basis set yields relatively similar dipole moment changes irrespective of the method, and the greatest values are generally obtained with the largest (triple- ζ) augmented basis sets.

3.2. Multidimensional Anharmonic Calculations. The vibrationally averaged dipole moments obtained from the VCI anharmonic calculations for the ground and excited ν_3 states are summarized in Table 2. Generally, the VCI dipole moments are lower than those obtained in the single mode approximation. The difference is smallest for the ground vibrational state, about 0.05 D for all methods, but increases in the excited states. The $\nu = 0$ dipole moments are computed lower than those for the minimum energy structure, by ~ 0.02 D (DFT methods) and ~ 0.03 D (post-HF methods), in contrast to the single mode approximation, which systematically predicted greater vibrationally averaged dipole moments compared to the minimum energy structure. The most dramatic difference is predicted for the fourth ($\nu = 4$) excited state, where the VCI dipole moments are smaller, by approximately 0.25 D, than those obtained in the single mode approximation.

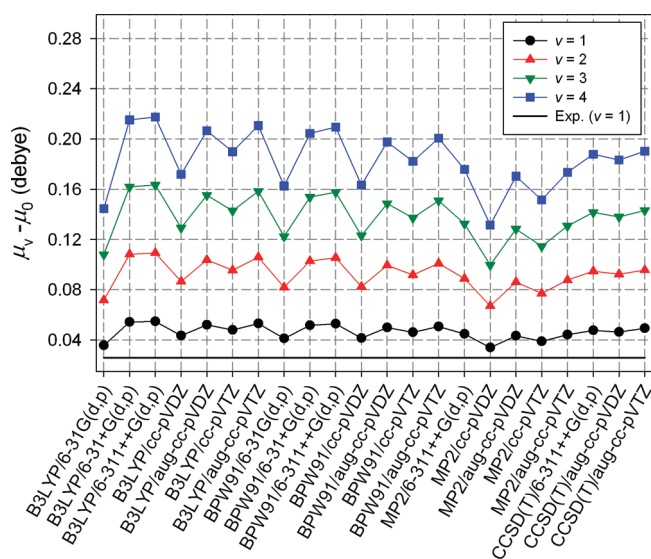
These differences are also reflected in trends with respect to the ν_3 vibrational state, as can be seen from Figure 4. Both DFT methods predict the dipole moment to increase up to $\nu = 3$, but the changes are significantly smaller than in the single mode approximation (Figures 2 and 3). The MP2 and CCSD(T) on the other hand yield a slightly smaller dipole moment for $\nu = 2$ than that for $\nu = 1$. While the gas-phase experimental dipole moment for $\nu = 2$ is not available, from the oH_2 -induced frequency shifts in pH_2 matrix experiments¹⁸ (also see below) it is evident that the dipole moment increases compared to the $\nu = 1$ (and $\nu = 0$) states. These qualitatively incorrect MP2 and CCSD(T) results may be explained by more anharmonic energy

Table 1. Vibrationally Averaged Dipole Moments (in D) for the ν_3 (C=O Stretch) Vibrational States in *trans*-FA in Single Mode Approximation

level	equilibrium	$\nu = 0$	$\nu = 1$	$\nu = 2$	$\nu = 3$	$\nu = 4$
B3LYP/6-31G(d,p)	1.4426	1.4601	1.4958	1.5318	1.5681	1.6047
B3LYP/6-31+G(d,p)	1.5315	1.5589	1.6132	1.6671	1.7207	1.7741
B3LYP/6-311++G(d,p)	1.4988	1.5245	1.5792	1.6337	1.6879	1.7419
B3LYP/cc-pVDZ	1.4243	1.4459	1.4894	1.5325	1.5753	1.6178
B3LYP/cc-pVTZ	1.5288	1.5755	1.6275	1.6793	1.7308	1.7821
B3LYP/aug-cc-pVDZ	1.5106	1.5346	1.5825	1.6302	1.6775	1.7245
B3LYP/aug-cc-pVTZ	1.5463	1.5710	1.6240	1.6768	1.7294	1.7817
BPW91/6-31G(d,p)	1.4181	1.4385	1.4797	1.5204	1.5609	1.6010
BPW91/6-31+G(d,p)	1.4867	1.5124	1.5640	1.6152	1.6661	1.7168
BPW91/6-311++G(d,p)	1.4592	1.4854	1.5383	1.5908	1.6430	1.6950
BPW91/cc-pVDZ	1.4026	1.4231	1.4645	1.5055	1.5461	1.5864
BPW91/cc-pVTZ	1.4911	1.5273	1.5771	1.6266	1.6759	1.7249
BPW91/aug-cc-pVDZ	1.4728	1.4957	1.5418	1.5875	1.6328	1.6779
BPW91/aug-cc-pVTZ	1.4984	1.5235	1.5742	1.6244	1.6744	1.7241
MP2/6-311++G(d,p)	1.3222	1.3440	1.3888	1.4329	1.4765	1.5197
MP2/cc-pVDZ	1.2763	1.2928	1.3266	1.3598	1.3923	1.4243
MP2/cc-pVTZ	1.3866	1.4059	1.4447	1.4828	1.5204	1.5574
MP2/aug-cc-pVDZ	1.4215	1.4426	1.4859	1.5286	1.5709	1.6129
MP2/aug-cc-pVTZ	1.4329	1.4557	1.4997	1.5433	1.5864	1.6291
CCSD(T)/6-311++G(d,p)	1.3307	1.3508	1.3981	1.4453	1.4921	1.5385
CCSD(T)/aug-cc-pVDZ	1.4281	1.4474	1.4938	1.5397	1.5854	1.6301
CCSD(T)/aug-cc-pVTZ	1.4041	1.4201	1.4693	1.5157	1.5632	1.6104
BPW91/cc-pVDZ/CPCM(Ar)	1.5583	1.5802	1.6256	1.6708	1.7156	1.7600
BPW91/cc-pVDZ/CPCM(pH ₂)	1.5160	1.5348	1.5693	1.6046	1.6404	1.6766
experiment (gas phase) ^a	—	1.4253	1.4512	—	—	—

^a Reference 8.**Figure 2.** Dipole moments calculated in single mode approximation at various levels of theory for ground ($\nu = 0$, black circles) and excited ($\nu = 1$, red triangles; $\nu = 2$, pink triangles; $\nu = 3$, green squares; and $\nu = 4$, blue diamonds) ν_3 vibrational states. Experimental values for $\nu = 0$ (black) and $\nu = 1$ (red) are shown as solid lines.

surfaces resulting from the wave function methods, compared to the DFT.^{24,45} The limited VCI based on the post-HF calculations may therefore not be adequate even for the vibrational quantum numbers as low as $\nu = 2$. From $\nu = 2$ to $\nu = 3$ all methods compute a significant increase, followed by a rather dramatic decrease of the dipole moment from $\nu = 3$ to $\nu = 4$ vibrational states. These nonuniform trends, contrasting the fairly systematic single mode results, are particularly apparent from the difference dipole moment values (with respect to $\nu = 0$) in Figure 4b.

**Figure 3.** Difference dipole moments (with respect to $\nu = 0$) calculated in the single mode approximation at various levels of theory for excited ν_3 vibrational states ($\nu = 1$, black circles; $\nu = 2$, red triangles; $\nu = 3$, green triangles; and $\nu = 4$, blue squares) with respect to the ground state. The experimental value (for $\nu = 1$) is shown as a solid black line.

In comparison with experiment, the B3LYP/6-311++G(d,p) calculated dipole moments are too large, while those obtained with the other methods, in particular the post-HF, are too small (Figure 4a). The BPW91/cc-pVDZ values fall in between and, while lower than experiment, are again in the closest agreement. These results are consistent with the single mode approximation at the same levels of theory. Comparing the relative values of the first excited vibrational state ($\nu = 1$) dipole moments with respect to $\nu = 0$ (Figure 4b), the B3LYP/6-311++G(d,p) calculation almost exactly repro-

duces the experimental difference. The BPW91/cc-pVDZ, MP2/6-311++G(d,p), and CCSD(T)/6-311++G(d,p) all underestimate the dipole moment increase. This is again in contrast with the single mode results, where all the calculations systematically overestimated the experimental differences.

In the simulated solid matrices, an increase of ~ 0.17 D in Ar and ~ 0.12 D in pH₂ with respect to the gas phase is predicted for all vibrational states. These changes are nearly identical to the single mode results, only slightly larger, and again approximately correspond to the changes in the equilibrium structure dipole moments due to the reaction field of the matrix. Unlike the single mode calculations, however, the VCI differences between the gas and matrix phases show a slight increase, rather than decrease, with the vibrational quantum number.

3.3. Effects of Residual oH₂ Clustering in pH₂ Matrices. Finally, we return to the original motivation for this computational study: modeling the IR spectral frequency shifts due to the clustering of quadrupolar oH₂ to the FA in pH₂ matrix.¹⁸ The interaction between the quadrupolar oH₂ and FA can be expressed as

$$V_{\text{dq}}(R, \theta_1, \theta_2, \varphi) = \frac{3\mu_1\Theta_2}{2R^4} [\cos \theta_1 (3 \cos^2 \theta_2 - 1) + 2 \sin \theta_1 \sin \theta_2 \cos \theta_2 \cos \varphi] \quad (12)$$

where μ_1 is the dipole moment of molecule “1” (FA), Θ_2 the quadrupole moment of molecule “2” (oH₂, 0.194116 au), the angles are assumed to correspond to the minimum energy configuration ($\theta_1 = \theta_2 = \varphi = 0$), and $R = 3.79$ Å, the nearest neighbor spacing of the pH₂ crystal. Note that the minimum energy configuration refers to the orientation of the electric moments rather than a particular orientation of the oH₂ and FA molecules: the oH₂ quadrupole moment arises from the $J = 1$ state and therefore is inherently averaged over the $J = 1$ rotational wave function.

In the original paper,¹⁸ the single mode BPW91/cc-pVDZ dipole moments computed in the gas phase were used to estimate the oH₂-induced frequency shifts. In the present study, the matrix effects were included using CPCM solvent model at a BPW91/cc-pVDZ level, which is computationally inexpensive and, as shown above, yields perhaps the best overall agreement with the gas phase as well as Ar and pH₂ matrix experimental data. Both single mode and VCI anharmonic calculations were performed, which allow us to reexamine the earlier results. Comparison with the experi-

Table 2. VCI Dipole Moments (in D) for the ν_3 (C=O stretch) Vibrational States in *trans*-FA

level	equilibrium	$\nu = 0$	$\nu = 1$	$\nu = 2$	$\nu = 3$	$\nu = 4$
B3LYP/6-311++G(d,p)	1.4988	1.4791	1.5044	1.5199	1.5488	1.4912
BPW91/cc-pVDZ	1.4026	1.3779	1.3884	1.4059	1.4158	1.3623
MP2/6-311++G(d,p)	1.3222	1.2893	1.2952	1.2915	1.3120	1.2688
CCSD(T)/6-311++G(d,p) ^a	1.3534	1.3270	1.3588	1.3422	1.3817	1.3139
BPW91/cc-pVDZ/CPCM(Ar)	1.5583	1.5422	1.5579	1.5716	1.5898	1.5306
BPW91/cc-pVDZ/CPCM(pH ₂)	1.5160	1.4945	1.5103	1.5244	1.5408	1.4776
experiment (gas phase) ^b	—	1.4253	1.4512	—	—	—

^a Molecular dipole moment calculated at the CCD/6-311++G(d,p) level. ^b Reference 8.

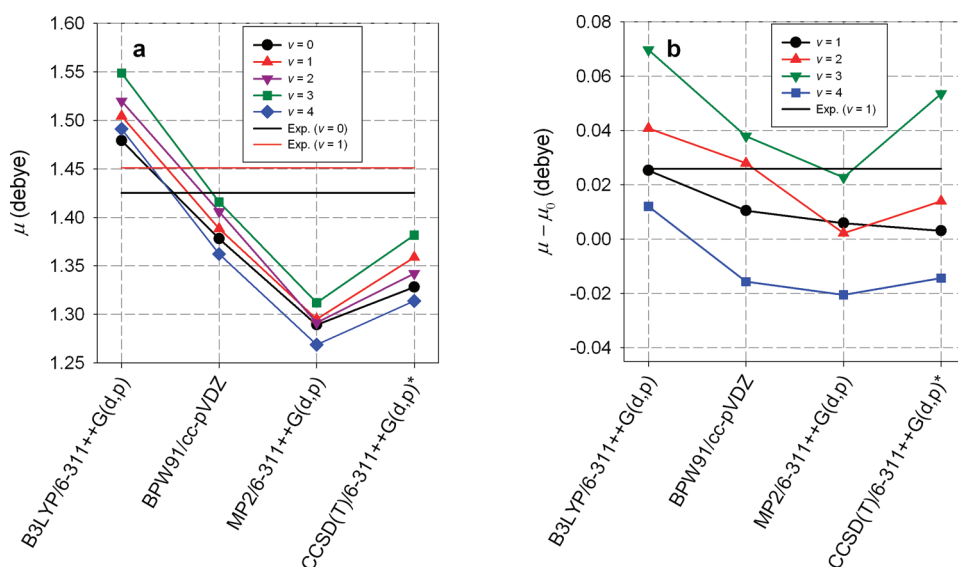


Figure 4. Dipole moments for ν_3 vibrational states of *trans*-FA calculated by VCI at various levels of theory. (a) Absolute dipole moments for the ground ($\nu = 0$, black circles) and excited ($\nu = 1$, red triangles; $\nu = 2$, pink triangles; $\nu = 3$, green squares; and $\nu = 4$, blue diamonds) ν_3 vibrational states calculated in single mode approximation at various levels of theory. Experimental values for $\nu = 0$ (black) and $\nu = 1$ (red) are shown as solid lines. (b) Difference dipole moments in excited ν_3 vibrational states ($\nu = 1$, black circles; $\nu = 2$, red triangles; $\nu = 3$, green triangles; and $\nu = 4$, blue squares) with respect to the ground state. Experimental value ($\nu = 1$) is shown as a solid black line.

Table 3. Interaction Energies (V_{dq}) and Frequency Shifts (Δ) Due to Quadrupole-Dipole Interaction between oH_2 and *trans*-FA in Ground and Excited ν_3 (C=O Stretch) Vibrational States

state	gas phase				CPCM pH_2				experiment: ^a Δ_{exp} (cm^{-1})
	single mode		VCI		single mode		VCI		
	V_{dq} (cm^{-1})	Δ (cm^{-1})	V_{dq} (cm^{-1})	Δ (cm^{-1})	V_{dq} (cm^{-1})	Δ (cm^{-1})	V_{dq} (cm^{-1})	Δ (cm^{-1})	
$\nu = 0$	27.28		26.41		29.42		28.86		
$\nu = 1$	28.07	-0.79	26.61	-0.19	30.08	-0.66	28.95	-0.30	-0.32
$\nu = 2$	28.86	-1.58	26.95	-0.54	30.79	-1.37	29.22	-0.57	-0.66

^a Reference 18.

mentally observed frequency shifts due to oH_2 clustering also provides an additional, albeit indirect, experimental check of the computed dipole moments.

Interaction potentials for $\nu = 0, 1,$ and $2 \nu_3$ vibrational states (eq 12) and the estimated oH_2 -induced frequency shifts are summarized in Table 3. For comparison, the corresponding gas-phase results and experimentally observed frequency shifts are also included. The gas-phase dipole moments calculated in the single mode approximation yield frequency shifts that are considerably higher, while the VCI somewhat lower, than the experiment. This reflects the differences between the excited and ground vibrational state dipole moments computed by the single mode and VCI methods (Figures 3 and 4b). With the pH_2 matrix, approximated by the CPCM model, the single mode frequency shifts become smaller, while the VCI ones increase. Both result in better agreement with the experimental values, despite the qualitatively opposite effect of the matrix. This is a consequence of the subtle differences in the influence of the pH_2 reaction field on the dipole moments in the ground and vibrationally excited states: the VCI with the CPCM gives slightly steeper dipole moment dependence on the vibrational excitation than the corresponding gas-phase calculation, while the opposite is true for the single mode treatment. Therefore, it appears that CPCM indeed improves the experimental frequency shift prediction; however, given the very small magnitude of these changes and inaccuracies of the computational methods, these results have to be regarded with caution.

4. Discussion

The vibrationally averaged dipole moments obtained using two different approximations, the single mode and VCI anharmonic calculations, reveal some systematic differences. For example, the dipole moments from the VCI calculations are consistently lower than the single mode results. The single mode treatment also uniformly predicts a greater increase of the dipole moment with vibrational excitation than VCI. Comparison of the anharmonic frequencies and IR intensities, presented in the Supporting Information, also shows that the VCI yields systematically lower fundamental and first overtone ν_3 frequencies and infrared intensities (Supporting Information, Tables S6–S9). On the other hand, for the higher overtones the VCI predict higher vibrational frequencies, and a reversal in the relative intensities is also observed for the third ν_3 overtone. The overall agreement with the available experimental data, including frequencies and IR absorption intensities,^{6–18} is, however, comparable for both the single mode and VCI approaches and is more signifi-

cantly dependent on the particular level of theory used in the calculation. The VCI calculations tend to agree better with the experimental frequencies and intensities (Supporting Information), especially for the fundamental transitions. The single mode calculations, by contrast, give closer agreement with the experimental dipole moments.

The fundamental assumption of the single mode method is that the vibrational motion follows the normal mode coordinate, which is equivalent to the neglect of interactions with the other normal modes. Although the ν_3 is not expected to strongly interact with the other modes, since it is localized and energetically well separated from other transitions, it is likely that the single mode picture breaks down for higher excited vibrational states. To estimate the validity of the local mode assumption, we examine the dependence of the molecular dipole moment on the vibrational quantum number ν . For an isolated mode the dipole moment increases linearly with the vibrational state.⁴⁶ In fact, this linearity has been used as evidence for the local character of the OH stretching in HOCl ⁴⁶ and H_2O .^{47,48} Therefore, it is not surprising that at all levels of theory the single mode treatment yields a near-perfect linear fit of the vibrationally averaged dipole moment as a function of the vibrational state (ν) with correlation coefficients better than 0.9999. Linear extrapolation from the calculated dipole moments for the ground ($\nu = 0$) and first excited ($\nu = 1$) states to $\nu = 2, 3,$ and 4 predicts the actual computed dipole moments to better than 0.0009 D for $\nu = 2$, 0.0022 D for $\nu = 3$, and 0.004 D for $\nu = 4$. Therefore, if the single mode approximation were valid, this near-perfect linear relationship would allow a straightforward estimation of the true dipole moments based on the known experimental values for the ground and first excited ν_3 vibrational states of FA (Table 1). With the most conservative estimation of the error, these values would be 1.4771 ± 0.0009 D for $\nu = 2$, 1.503 ± 0.002 D for $\nu = 3$, and 1.529 ± 0.004 D for $\nu = 4$.

Examination of the linearity of this relationship predicted by the VCI anharmonic calculations provides an independent test for the “locality” of the C=O stretching mode. Unfortunately, the dipole moment dependence on ν in the VCI calculations varies widely, depending on the level of theory used. The DFT methods yield a very good linear relationship for $\nu = 0, 1, 2,$ and 3 with the correlation coefficient of 0.994 for both B3LYP/6-311++G(d,p) and BPW91/cc-pVDZ. On the other hand, for the post-HF levels, there is hardly any linear trend. This qualitative inconsistency illustrates that the VCI method is also subject to inherent approximations and errors. The truncated Taylor expansions

Table 4. Dipole Moments (in D) for the ν_3 (C=O Stretch) Vibrational States in *trans*-FA in Single Mode Approximation, with the Correction for the ZPE States of the Remaining Modes and from VCI Anharmonic Theory at the BPW91/cc-pVDZ Level

method	$\nu = 0$	$\nu = 1$	$\nu = 2$	$\nu = 3$	$\nu = 4$
single mode	1.4231	1.4645	1.5055	1.5461	1.5864
single mode ZPE corrected	1.3935	1.4349	1.4759	1.5165	1.5568
anharmonic VCI	1.3779	1.3884	1.4059	1.4158	1.3623
experiment (gas phase) ^a	1.4253	1.4512	–	–	–

^a Reference 8.

of the potential energy (eq 7) and dipole moment (eq 9) are expected to introduce errors, especially for higher excited vibrational states, which are more sensitive to the energy and dipole surfaces further away from the energy minimum. Moreover, the limited harmonic oscillator basis (to states where the sum of quantum numbers for all modes is less or equal to five) will also likely affect the results for the higher vibrationally excited state properties.

We have tested the convergence of the dipole moment values for $\nu = 0$ to $\nu = 4$ vibrational states, obtained with BPW91/cc-pVDZ parameters, with the size of the VCI harmonic basis, which included from four up to seven excited state wave functions (Supporting Information, Table S3). While the dipole moments in all vibrational states are somewhat dependent on the harmonic basis size, up to $\nu = 3$ the computed values are essentially stable. The $\nu = 4$ dipole moment, as might be expected, is the most sensitive to inclusion of additional basis functions. The qualitative trend of the decrease in the dipole moment from $\nu = 3$ to $\nu = 4$, however, is not affected. Furthermore, the larger the harmonic basis, the more significantly the $\nu = 4$ vibrational state becomes mixed with other harmonic modes. For example, with the largest harmonic basis tested, including up to seven excited harmonic functions, the contribution of the ν_3 normal mode to the VCI anharmonic wave function is only 27%. As a consequence, the $\nu = 4$ vibrational state can no longer be considered a pure ν_3 mode, which is consistent with the breakdown of the linear dependence of the dipole moment on the vibrational quantum number.

All combined, it is apparent that the fourth ($\nu = 4$) excited vibrational state cannot likely be treated as an isolated mode and the single mode approximation cannot be expected to yield reliable dipole moment values. On the other hand, as suggested by the DFT VCI results, up to $\nu = 3$ the approximation may hold, in which case the above prediction for the gas-phase $\nu = 2$ and $\nu = 3$ dipole moments in the neighborhood of 1.48 and 1.50 D, respectively, should be valid. The experimental study of the dipole moments of OH stretching vibrational states in HOCl⁴⁶ and H₂O⁴⁷ found the single (local) mode picture to hold up to $\nu = 4$. Furthermore, based on the comparison of the VCI calculations at different theory levels and the convergence tests with the size of the harmonic basis, it is also unlikely that the multidimensional VCI results are reliable for $\nu = 4$. Neither of the two

approaches, therefore, appears well-suited for computing molecular properties for highly excited vibrational states ($\nu > 3$).

Interaction and mixing of the individual normal modes is only one of several potential problems associated with the single mode approximation. Even in the complete absence of intermode coupling, this treatment neglects the contribution of the zero point energy (ZPE) states of the remaining (anharmonic) modes to the property of interest, in this case the dipole moment. In order to estimate this effect, we keep the assumption of the noninteracting, separable normal modes, which allows writing the total wave function as a product of the one-dimensional functions

$$|\Psi(R_1, R_2, \dots, R_N)\rangle = |\psi_{\nu_1}(R_1)\psi_{\nu_2}(R_2)\dots\psi_{\nu_N}(R_N)\rangle \quad (13)$$

where R_i is the normal coordinate (non-mass-weighted), as above. The applicability of the single mode approximation for calculation of the dipole moment also requires a separable dipole moment operator

$$\mu(R_1, R_2, \dots, R_N) = \mu_1(R_1) + \mu_2(R_2) + \dots + \mu_N(R_N) \quad (14)$$

i.e., all derivatives of the type ($\partial^2\mu/\partial R_i\partial R_j$) in the Taylor expansion of the dipole moment are negligible for $i \neq j$. This, to some extent, resembles the “second harmonic approximation” used in calculation of absorption intensities in the (harmonic) vibrational spectra. The dipole moment expansion, however, is not truncated at the linear term; only the cross derivatives are neglected:

$$\begin{aligned} \mu_\alpha &= \mu_{0,\alpha} + \sum_i \left(\frac{\partial\mu_{i,\alpha}}{\partial R_i} R_i + \frac{1}{2} \frac{\partial^2\mu_{i,\alpha}}{\partial R_i^2} R_i^2 + \frac{1}{3!} \frac{\partial^3\mu_{i,\alpha}}{\partial R_i^3} R_i^3 + \dots \right) \\ &= \mu_{0,\alpha} + \sum_i (\mu_{i,\alpha} - \mu_{0,\alpha}) \end{aligned} \quad (15)$$

where $\alpha = \{x, y, z\}$ and μ_0 is the minimum energy structure (equilibrium) dipole moment. Then the ZPE-corrected dipole moment for the ν_3 (C=O stretch) vibrational state ν is

$$\mu_\alpha(\nu_3) = \mu_{\alpha,0} + \langle \psi_\nu(R_{\nu_3}) | \mu_{\nu_3,\alpha} - \mu_{0,\alpha} | \psi_\nu(R_{\nu_3}) \rangle + \sum_{i \neq \nu_3} \langle \psi_0(R_i) | \mu_{i,\alpha} - \mu_{0,\alpha} | \psi_0(R_i) \rangle \quad (16)$$

Under these assumptions, the contribution of the additional normal modes can be evaluated using only 1D potential energy surfaces for each mode. It must be stressed, however, that assumptions analogous to those made for ν_3 are not automatically valid for all normal modes. Especially the highly anharmonic, low frequency vibrations may not be separable.

For this “ZPE-corrected” single mode approximation, we have calculated the potential energy and dipole moments as functions of normal coordinate displacements for all nine normal modes of FA at the BPW91/cc-pVDZ level (Supporting Information, Table S4). In analogy to the computations of the vibrationally averaged dipole moments for the ν_3 as described in Computational Methods, the vibrational

wave functions for each mode can be obtained and substituted into eq 16. In Table 4, we compare the vibrationally averaged BPW91/cc-pVDZ dipole moments computed for the local ν_3 mode only (eq 6, Table 1) with those including the ZPE correction for all vibrational modes (eq 16).

The ZPE contribution of the remaining modes causes a noticeable decrease in the ν_3 vibrationally averaged dipole moments by approximately 0.03 D for all states. The shift towards lower dipole moment values, although relatively small ($\approx 2\%$), is qualitatively consistent with the BPW91/cc-pVDZ VCI anharmonic results, for convenience also shown in Table 4. The ground vibrational state dipole moment for the ZPE-corrected single mode is just ~ 0.015 D greater than the VCI anharmonic result, but also more than 0.03 D lower than the experimental dipole. The differences with respect to the VCI calculations increase for the excited states due to a steeper dependence of the single mode dipole moment on the vibrational state (Figures 2 and 4), which is obviously unaffected by the correction. The $\nu = 1$ dipole moment is also lower than the experiment, but the error is approximately equal to the noncorrected single mode calculation.

The ZPE contribution also accounts, at least in part, for one of the discrepancies between the single mode and VCI calculations as to whether the vibrationally averaged dipole moment for the ground ν_3 state is smaller (VCI calculations) or greater (single mode calculations) than the equilibrium (minimum energy) structure. The ZPE-corrected single mode dipole moment value becomes lower than that computed for the minimum energy structure (1.4026 D).

We note that the single mode treatment of all vibrational modes also gives, within this approximation, the vibrational frequencies and intensities of the fundamental and overtone transitions for all nine vibrational modes of FA. These results are presented in the Supporting Information (Tables S10 and S11) and compared with the experimental data (as well as with the VCI calculations) to provide additional tests for the performance of the single mode approximation at the BPW91/cc-pVDZ level. In addition, vibrationally averaged dipole moments for the excited vibrational states of all vibrational modes can be obtained. For reference, we present the computed dipole moments for the first excited vibrational states ($\nu = 1$) (Supporting Information, Table S4) along with the full anharmonic VCI results (Supporting Information, Table S5).

Our calculations have also provided tests for the performance of different levels of theory, including DFT, post-HF correlated wave function methods, and a number of basis sets. The errors in the computed molecular properties at different levels of theory as compared to experiment are reflected in both single mode and VCI anharmonic calculations, and some systematic trends can be inferred. For example, with the same basis sets, the post-HF dipole moments are uniformly smaller than those from the DFT. These trends are already apparent from the dipole moments within the harmonic approximation. As a consequence, with smaller basis sets the DFT yields dipole moments closer to experiment, while the post-HF ones are too low. With larger basis, however, in particular the correlation consistent basis

sets augmented with diffuse functions, the calculated dipole moment values systematically increase and the post-HF predictions improve relatively to the DFT ones, which become much too large.

One of the interesting results was a surprisingly good overall performance of the BPW91/cc-pVDZ level. We have used this particular level of theory previously in simulations of the vibrational amide I (predominantly amide C=O stretch) spectra of model amides, since it appeared to give the best agreement of the harmonic vibrational frequency with the experimental gas-phase value for *N*-methylacetamide (NMA).^{20–22} In this study, within the single mode approximation, we obtained the best agreement between BPW91/cc-pVDZ calculations with experiment for the dipole moments as well as the frequencies and IR intensities (Supporting Information). In the anharmonic VCI calculations, the agreement of both the predicted frequencies and dipole moments with experiment is worse, but still remarkably good in comparison with the other levels tested.

The unusually good performance of BPW91/cc-pVDZ must be due to a fortuitous cancellation of errors of the density functional and the basis set. The results obtained with the BPW91 systematically differ from those computed with the other methods: e.g., the harmonic vibrational frequencies are systematically lower (Supporting Information, Table S6). On the other hand, the cc-pVDZ basis set with all the computational methods produces higher vibrational frequencies than any other basis except 6-31G(d,p). These errors seem to compensate for each other very well in the combination BPW91/cc-pVDZ. With larger basis sets BPW91 tends to underestimate the vibrational frequencies, while for the other methods as the computed frequencies become lower with increasing basis set size, the agreement with experiment improves. For dipole moments, the BPW91 results are not as dramatically different from the other methods but fall in between the higher B3LYP values and the too low post-HF ones. The cc-pVDZ basis, however, again gives systematically the lowest dipole moments. While MP2 with this basis yields dipole moments that are much too small compared to the experiment and B3LYP/cc-pVDZ dipoles are systematically too high, the BPW91/cc-pVDZ-calculated dipole again falls very close to the experimental value. Thus, on an empirical basis, the BPW91/cc-pVDZ level of theory appears as a useful and computationally cheap model for the vibrational properties of the carbonyl group.

5. Conclusion

The explanation of multiple closely spaced peaks of the *trans*-FA ν_3 band in low-temperature, solid p H_2 required a reliable estimate of dipole moments in different ν_3 vibrational states. Calculations of vibrationally averaged molecular dipole moments represent a challenge, in particular for higher vibrationally excited vibrational states. We have tested two different methodologies: the single mode treatment and multidimensional limited VCI calculations. With both methods, very good results for the ground and first excited state dipole moments were obtained; however, the reliability of the predictions for higher excited states is difficult to verify. The linearity of the dipole moment as a function of

vibrational energy quanta, independently obtained from the VCI calculations at two DFT levels, suggests that the single mode picture is valid up to the third excited state ($v = 3$). Apart from the breakdown of the single mode picture due to combination with other normal modes and/or nonseparability of the dipole operator, the single mode approximation also neglects the zero point contribution of the remaining modes to the vibrationally averaged dipole moment. This contribution is non-negligible and the resulting dipole moments more closely correspond to those obtained from VCI. Unfortunately, even the VCI calculations are unlikely to be reliable for highly excited vibrational state properties, due in part to the anharmonic corrections based on the truncated Taylor series and in part to the truncation of the VCI harmonic basis, dictated by the computational cost of the VCI calculation. Of the different computational levels tested, we found the BPW91/cc-pVDZ to give remarkably good overall performance. In general, DFT results, while quite close with smaller basis sets, seem to depart increasingly from the experiment upon increasing the basis set size. In contrast, post-HF methods, while requiring large basis sets, appear to converge to better agreement with the available experimental data. A more detailed evaluation of the performance of different computational methods remains difficult due to the scarcity of the dipole moment experimental data. However, the results demonstrate that the computational methodology provides robust tools for studies of the molecular electrostatic properties in various vibrational states as well as interactions with the environment. In particular, the predicted vibrationally averaged dipole moments well-explained the quadrupole-dipole splitting of the IR lines of the FA in the solid pH₂ matrix.

Acknowledgment. This work was supported in part by the National Science Foundation CAREER: 0846140 grant to J.K., Grant Agency of the Czech Republic (202/07/0732, to P.B.), and the Grant Agency of the Academy of Sciences (A400550702, M200550902, to P.B. and J.K.).

Supporting Information Available: Anharmonic vibrationally averaged structural parameters, convergence of VCI dipole moments with the size of harmonic basis, potential energy surfaces and dipole moment functions for additional levels of theory, single mode and VCI vibrational frequencies and absorption intensities, dipole moments for all FA normal modes in single mode approximation, and VCI dipole moments for singly excited FA vibrational states. This information is available free of charge via the Internet at <http://pubs.acs.org>.

References

- (1) Stone, A. J. *The Theory of Intermolecular Forces (International Series of Monographs on Chemistry)*; Oxford University Press: New York, 1997; pp 36–49.
- (2) Craig, D. P.; Thirunamachandran, T. *Molecular quantum electrodynamics*; Dover Publications: New York, 1998; pp 142–182.
- (3) Onsager, L. *J. Am. Chem. Soc.* **1936**, *58*, 1486.
- (4) Reichardt, C. *Solvents and Solvent Effects in Organic Chemistry*, 3rd ed.; Wiley-VCH: New York, 2003; pp 329–388.
- (5) Nigam, S.; Rutan, S. *Appl. Spectrosc.* **2001**, *55*, 362A.
- (6) Redington, R. L. *J. Mol. Spectrosc.* **1977**, *65*, 171.
- (7) Marèchal, Y. *J. Chem. Phys.* **1987**, *87*, 6344.
- (8) Weber, W. H.; Maker, P. D.; Johns, J. W. C.; Weinberger, E. *J. Mol. Spectrosc.* **1987**, *121*, 243.
- (9) Hurtmans, D.; Herregodts, F.; Herman, M.; Lievin, J.; Campargue, A.; Garnache, A.; Kachanov, A. A. *J. Chem. Phys.* **2000**, *113*, 1535.
- (10) Freytes, M.; Hurtmans, D.; Kassi, S.; Lievin, J.; Auwera, J. V.; Campargue, A.; Herman, M. *Chem. Phys.* **2002**, *283*, 47.
- (11) Lundell, J.; Rasanen, M.; Latajka, Z. *Chem. Phys.* **1994**, *189*, 245.
- (12) Pettersson, M.; Lundell, J.; Khriachtchev, L.; Rasanen, M. *J. Am. Chem. Soc.* **1997**, *119*, 11715.
- (13) Madeja, F.; Markwick, P.; Havenith, M.; Nauta, K.; Miller, R. E. *J. Chem. Phys.* **2002**, *116*, 2870.
- (14) Macoas, E. M. S.; Lundell, J.; Pettersson, M.; Khriachtchev, L.; Fausto, R.; Rasanen, M. *J. Mol. Spectrosc.* **2003**, *219*, 70.
- (15) Marushkevich, K.; Khriachtchev, L.; Rasanen, M. *J. Chem. Phys.* **2007**, *126*, 241102.
- (16) Marushkevich, K.; Khriachtchev, L.; Rasanen, M. *Phys. Chem. Chem. Phys.* **2007**, *9*, 5748.
- (17) Olbert-Majkut, A.; Ahokas, J.; Lundell, J.; Pettersson, M. *Chem. Phys. Lett.* **2009**, *468*, 176.
- (18) Paulson, L. O.; Anderson, D. T. *J. Phys. Chem. A* **2009**, *113*, 1770.
- (19) Nyquist, R. A. *Appl. Spectrosc.* **1986**, *40*, 336.
- (20) Kubelka, J.; Keiderling, T. A. *J. Phys. Chem. A* **2001**, *105*, 10922.
- (21) Amunson, K. E.; Kubelka, J. *J. Phys. Chem. B* **2007**, *111*, 9993.
- (22) Ackels, L.; Stawski, P.; Amunson, K. E.; Kubelka, J. *Vib. Spectrosc.* **2008**, *50*, 2.
- (23) Bouř, P. *J. Chem. Phys.* **2004**, *121*, 7545.
- (24) Andrushchenko, V.; Matějka, P.; Anderson, D. T.; Kaminský, J.; Horníček, J.; Paulson, L. O.; Bouř, P. *J. Phys. Chem. A* **2009**, *113*, 9727.
- (25) Daněček, P.; Bouř, P. *J. Comput. Chem.* **2007**, *28*, 1617.
- (26) Takahashi, K.; Sugawara, M.; Yabushita, S. *J. Phys. Chem. A* **2002**, *106*, 2676.
- (27) Wallace, R. *Chem. Phys.* **1975**, *11*, 189.
- (28) Swofford, R. L.; Long, M. E.; Albrecht, A. C. *J. Chem. Phys.* **1976**, *65*, 179.
- (29) Takahashi, K.; Sugawara, M.; Yabushita, S. *J. Phys. Chem. A* **2003**, *107*, 11092.
- (30) Takahashi, K.; Sugawara, M.; Yabushita, S. *J. Phys. Chem. A* **2005**, *109*, 4242.
- (31) Henry, B. R. *Acc. Chem. Res.* **1977**, *10*, 207.
- (32) Lemus, R.; Frank, A. *Int. J. Quantum Chem.* **1999**, *75*, 465.
- (33) Jensen, P. *Mol. Phys.* **2000**, *98*, 1253.

- (34) Daněček, P.; Kapitán, J.; Baumruk, V.; Bednářová, L.; Kopecký, V.; Bouř, P. *J. Chem. Phys.* **2007**, *126*, 224513.
- (35) Dračínský, M.; Kaminský, J.; Bouř, P. *J. Chem. Phys.* **2009**, *130*, 094106.
- (36) Frisch, M. J.; Trucks, G. W.; Schlegel, H. B.; Scuseria, G. E.; Robb, M. A.; Cheeseman, J. R.; Zakrzewski, V. G.; Montgomery, J., J. A.; Stratmann, R. E.; Burant, J. C.; Dapprich, S.; Millam, J. M.; Daniels, A. D.; Kudin, K. N.; Strain, M. C.; Farkas, O.; Tomasi, J.; Barone, V.; Cossi, M.; Cammi, R.; Mennucci, B.; Pomelli, C.; Adamo, C.; Clifford, S.; Ochterski, J.; Petersson, G. A.; Ayala, P. Y.; Cui, Q.; Morokuma, K.; Malick, D. K.; Rabuck, A. D.; Raghavachari, K.; Foresman, J. B.; Cioslowski, J.; Ortiz, J. V.; Stefanov, B. B.; Liu, G.; Liashenko, A.; Piskorz, P.; Komaromi, I.; Gomperts, R.; Martin, R. L.; Fox, D. J.; Keith, T.; Al-Laham, M. A.; Peng, C. Y.; Nanayakkara, A.; Gonzalez, C.; Challacombe, M.; Gill, P. M. W.; Johnson, B.; Chen, W.; Wong, M. W.; Andres, J. L.; Gonzalez, C.; Head-Gordon, M.; Replogle, E. S.; Pople, J. A. *Gaussian 98; Revision A.6*; Gaussian, Inc.: Pittsburgh PA, 1998.
- (37) Barone, V.; Cossi, M. *J. Phys. Chem. A* **1998**, *102*, 1995.
- (38) Cossi, M.; Rega, N.; Scalmani, G.; Barone, V. *J. Comput. Chem.* **2003**, *24*, 669.
- (39) Wallace, B. A.; Meyer, H. J. *Low Temp. Phys.* **1974**, *15*, 297.
- (40) ACESII - Mainz-Austin-Budapest version: Stanton, J. F.; Gauss, J.; Watts, J. D.; Szalay, P. G.; Bartlett, R. J., with contributions from Auer, A. A.; Bernholdt, D. E.; Christiansen, O.; Harding, M. E.; Heckert, M.; Heun, O.; Huber, C.; Jonsson, D.; Jusélius, J.; Lauderdale, W. J.; Metzroth, T.; Michauk, C.; Price, D. R.; Ruud, K.; Schiffmann, F. Tajti, A.; Varner, M. E.; Vázquez, J. and the integral packages: MOLECULE (J. Almlöf and P. R. Taylor), PROPS (Taylor, P. R.), and ABACUS (Helgaker, T.; Jensen, H. J. Aa.; Jørgensen, P.; Olsen, J.).
- (41) Cerjan, C.; Kulander, K. C. *Comput. Phys. Commun.* **1991**, *63*, 529.
- (42) Sugawara, M.; Kato, M.; Fujimura, Y. *Chem. Phys. Lett.* **1991**, *184*, 203.
- (43) Bouř, P. *J. Phys. Chem.* **1994**, *98*, 8862.
- (44) Bouř, P.; Bednářová, L. *J. Phys. Chem.* **1995**, *99*, 5961.
- (45) Kapitán, J.; Hecht, L.; Bouř, P. *Phys. Chem. Chem. Phys.* **2008**, *10*, 1003.
- (46) Callegari, A.; Theule, P.; Schmied, R.; Rizzo, T. R.; Muentner, J. S. *J. Mol. Spectrosc.* **2003**, *221*, 116.
- (47) Shostak, S. L.; Ebenstein, W. L.; Muentner, J. S. *J. Chem. Phys.* **1991**, *94*, 5875.
- (48) Shostak, S. L.; Muentner, J. S. *J. Chem. Phys.* **1991**, *94*, 5883.

CT900608T